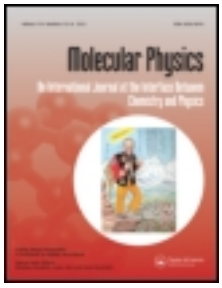

Molecular Physics: An International Journal at the Interface Between Chemistry and Physics

Publication details, including instructions for authors and subscription information:
http://www.tandfonline.com/loi/tmph20

Chaotic dynamics near steep transition states

Jason R. Green [a], Thomas S. Hofer [b], David J. Wales [c] & R. Stephen Berry [d]

[a] Department of Chemistry, Northwestern University, 2145 Sheridan Road, Evanston, IL 60208-3100, USA

[b] Theoretical Chemistry Division, Institute of General, Inorganic and Theoretical Chemistry, Leopold-Franzens-University of Innsbruck, Innrain 80-82, Innsbruck 6020, Austria

[c] Department of Chemistry, University of Cambridge, Lensfield Road, Cambridge, CB2 1EW, UK

[d] Department of Chemistry, The University of Chicago, Chicago, Illinois 60637, USA

Accepted author version posted online: 18 Apr 2012.Version of record first published: 11 May 2012.

To cite this article: Jason R. Green, Thomas S. Hofer, David J. Wales & R. Stephen Berry (2012): Chaotic dynamics near steep transition states, Molecular Physics: An International Journal at the Interface Between Chemistry and Physics, 110:15-16, 1839-1848

To link to this article: http://dx.doi.org/10.1080/00268976.2012.684894

Molecular Physics
Vol. 110, Nos. 15–16, 10–20 August 2012, 1839–1848

Taylor & Francis
Taylor & Francis Group

INVITED ARTICLE

Chaotic dynamics near steep transition states

Jason R. Green[a], Thomas S. Hofer[b], David J. Wales[c] and R. Stephen Berry[d]*

[a]*Department of Chemistry, Northwestern University, 2145 Sheridan Road, Evanston, IL 60208-3100, USA;* [b]*Theoretical Chemistry Division, Institute of General, Inorganic and Theoretical Chemistry, Leopold-Franzens-University of Innsbruck, Innrain 80-82, Innsbruck 6020, Austria;* [c]*Department of Chemistry, University of Cambridge, Lensfield Road, Cambridge, CB2 1EW, UK;* [d]*Department of Chemistry, The University of Chicago, Chicago, Illinois 60637, USA*

(*Received 31 December 2011; final version received 3 April 2012*)

Classical molecular motion near potential energy saddles can be more or less chaotic relative to motion near minima. The relative degree of chaos depends on the extent of coupling between the degrees of freedom and on the curvature of the potential energy landscape. Here, we explore these effects using constant energy molecular dynamics simulations and independent criteria associated with locally chaotic behavior – namely, the constancy of the local mode action and the magnitude of finite-time Lyapunov exponents. These criteria reconcile the chaotic basins and relatively ordered saddles of the Lennard-Jones trimer, with the chaotic saddles and ordered basins for reactive, all-atom H_2O described by the Garofalini H_2O potential. By modifying the Garofalini and Lennard-Jones models we separate the compounding effects of nonlinear three-body interactions and steep reaction path curvature on the local degree of chaos near saddles and minima.

Keywords: molecular dynamics; local chaos; reaction pathway; three-body interactions

1. Introduction

Theories of chemical reactions are centered around the transient states of molecules during their transformation from reactant to product. Classically, the full specification of a state is a point in position-momentum phase space; however, a common reduced description of the transition state is the potential energy saddle point connecting reactant and product minima. A minimal description of a reaction is then the union of the two steepest-descent paths connecting the transition state to the minima. However, this description does not account for the explicit dynamics involved in large-amplitude, coupled, irregular motions characteristic of isomerization or bond breaking. A proper dynamical account of the transition states involved is a true test of the unification of classical dynamics and statistical theories of reaction rates. Motivated by the development of statistical reaction rate theories, much work has focused on the *local* extent of dynamical coupling between the reaction coordinate and the remaining vibrational modes, beginning with studies by Miller [1] and Marcus [2].

Stationary points create narrow bottlenecks that control transport through some phase space regions [3–5]. The extent to which vibrations are adiabatic in these bottlenecks is connected to the anharmonic mode-mode coupling, potential energy curvature, and to the degree of dynamical instability or the convergence and divergence of trajectories [6–8]. The rate at which trajectories separate is measured by Lyapunov exponents [9,10]. One interesting aspect of dynamical instability near potential energy saddles that emerged from numerical simulations of atomic clusters was that some potential energy saddles induce more regular motion relative to their connecting minima than others [11–17]. Subsequent work, further analyzing the concept of local regularity, demonstrated the existence and persistence of local approximate invariants of the motion in the vicinity of a saddle point [18–20]. More recently, a mathematical framework has been established by Wiggins and coworkers [21,22], and Lorquet has examined the correlation between the regularity of dynamics and the "flatness" of the saddle along the reactive mode [23].

Recently, in numerical simulations of an isolated water molecule with a particular model potential, we discovered saddles that induce more chaotic motion than their connecting minima, as indicated by finite-time Lyapunov exponents [24]. The dynamics of water have been extensively studied in the past [25–28]; however, an interesting aspect of the model used in our work was that trajectories were dispersed, rather than collimated, in the vicinity of the saddle. This behavior was attributed to a stronger coupling of the degrees of

*Corresponding author. Email: berry@uchicago.edu

ISSN 0026–8976 print/ISSN 1362–3028 online

http://dx.doi.org/10.1080/00268976.2012.684894
http://www.tandfonline.com

freedom caused by three-body interactions in the model used. The steepness of the potential energy near the saddle along the reaction coordinate was also suspected to be a contributing factor, despite finding lower *total* curvature in the saddle than the minima. Here we explore this phenomenon further with independent measures of local chaos and numerical computation of the steepest-descent reaction paths. In this work a transition state will be considered "steep" if there is a high degree of curvature near the saddle point.

After introducing our simulation methods and the molecular models, we discuss our results for the chaotic dynamics of triatomics and the various influences on this behavior.

2. Model and methods

Dynamics are determined by features of the potential energy landscape, and to complement our classical trajectory simulations we identified the stationary points of several triatomic molecules and the corresponding isomerization mechanisms. For our atomistic simulations of the water molecule, we adopted the reactive, interatomic potential developed by Garofalini *et al*. [29], which allows the dynamics and dynamical instability of all classical degrees of freedom to be studied [30]. The potential is a three-center, reactive model for water involving three point charges and three diffuse (Gaussian) functions centered on the nuclei. It is entirely flexible, with full permutational symmetry, and it includes pair and three-body interactions; we refer to Garofalini *et al*.'s work for a full description of the model. Our comments will be restricted to the three-body contribution to the potential. To separate the effects of three-body interactions and the steep barrier on the dynamics we modified the Garofalini parameters, which had other benefits, to be discussed later.

The Lennard-Jones (LJ) trimer, 12–6 LJ_3, served as a reference, given the extensive work performed on this system in the past [31–33]. However, the Lennard-Jones potential is a special case of the Mie potential [34], which we used in the present study. The interaction of two particles k and j a distance r_{kj} apart modeled by the Mie potential is represented mathematically through the potential energy function

$$V(r_{kj}) = \varepsilon_{kj}\frac{n}{n-m}\left(\frac{n}{m}\right)^{\frac{m}{n-m}}\left[\frac{\sigma^n}{r_{kj}^n} - \frac{\sigma^m}{r_{kj}^m}\right].$$

Two parameter sets were selected for a three-atom cluster. One set of parameters with $n = 12$, $m = 6$, $\varepsilon = 1$, $\sigma = 1$ was equivalent to 12–6 LJ_3. Another set was chosen to approximate the isomerization pathway of Garofalini H_2O, with $n = 1.2$, $m = 2.1$, $\varepsilon \approx 3.6$, $\sigma \approx 0.60$, for what we will call the 2.1–1.2 Mie trimer.

Configurations corresponding to potential energy minima for Garofalini H_2O, modified Garofalini H_2O (still to be discussed), 12–6 LJ_3 and the 2.1–1.2 Mie trimer, were found by limited memory Broyden–Fletcher–Goldfarb–Shanno (L-BFGS) minimization [35]. Potential energy saddle configurations were located by a modified version of hybrid eigenvector-following [36–39] with a root-mean-square gradient termination criterion of $10^{-4}\,\mathrm{kcal\,mol^{-1}\,\AA^{-1}}$.

Numerical second derivatives of the potential energy were needed for several quantities of interest. These derivatives were computed using central differences of the analytical gradients with a displacement of 10^{-9} Å. Diagonalizing the mass-weighted Hessian matrix of these second derivatives gave the $3N-6$ unit eigenvectors $\{\hat{\mathbf{u}}_i\}$. At potential energy minimum and saddle configurations the eigenvectors are the normal mode vectors. At each time step along a trajectory these eigenvectors are the instantaneous or local normal modes. The $3N-6$ eigenvalues of the mass-weighted Hessian matrix $\{\omega_i^2\}$, the squares of the normal mode frequencies, were placed in ascending order: $\omega_1^2 \le \omega_2^2 \le \cdots \le \omega_{3N-6}^2$. The six remaining eigenvalues corresponding to overall translation and rotation were projected from the Hessian using standard techniques [40].

The stationary point normal modes serve two main purposes. First, normal mode vectors were used as displacements of (center-of-mass frame) global minimum equilibrium configurations to fix initial conditions for numerical trajectories. After displacement in normal mode directions, the potential energy fixed the total energy for the subsequent trajectory. Thus, the normal mode excitations were used to control the initial total energy. All the reported total energies are relative to the potential energy of the global minimum configuration. Second, the normal mode frequencies provided convenient reference points for the Lyapunov exponents. Our numerical methods for simulating Gram–Schmidt (Lyapunov) vectors and the computation of Lyapunov exponents have been described in detail elsewhere [41]. No translation-rotation projection was performed on the Hessians used for Gram–Schmidt vector propagation.

3. Results and discussion

Our previous investigation of the Garofalini water model revealed the existence of unphysical $C_{\infty v}$ saddles (asymmetric, linear configurations) in isolated

H_2O [24]. Also, the finite-time Lyapunov exponents calculated from simulated classical trajectories and Gram–Schmidt Lyapunov vectors indicated more chaotic motion near saddles and less chaotic motion near the minimum. This result was attributed to strong reaction coordinate-mode coupling in this model and the changes in potential energy curvature along the reaction coordinate. Coupling of the reaction coordinate, the bending vibrational mode, is a consequence of the bond length dependent angular forces in the three-body contributions to the potential. We will now explore this feature of the Garofalini model further, along with our modifications to the potential parameters that eliminate these forces and the additional saddles.

3.1. *Isomerization pathways of the Garofalini water potential*

The HOH three-body term U_3 in the Garofalini water model

$$U_3(\mathbf{r}_{ij}, \mathbf{r}_{ik}, \theta_{jik}) = \nu_{jik} e^{\frac{\gamma_{ij}}{\|\mathbf{r}_{ij}\| - r_{ij}^0}} e^{\frac{\gamma_{ik}}{\|\mathbf{r}_{ik}\| - r_{ik}^0}} \left[\cos\theta_{jik} - \cos\theta_{jik}^0\right]^2 \tag{1}$$

is a screened, cosine-harmonic angle with a cutoff r_{ij}^0 for the bond vectors $\mathbf{r}_{ij}$ and $\mathbf{r}_{ik}$. The HOH angle θ_{jik} between the bond vectors is constrained by the ideal angle θ_{jik}^0. The exponential factors modify or ''screen'' the interaction between the atoms i, j, and k depending on their deviation from the ideal angle θ_{jik}^0. The parameter ν_{jik} determines the strength of the three-body interactions as well as the isomerization barrier height. Mahadevan and Garofalini chose the parameters γ_{ij} and γ_{ik} such that ideal HOH angle is 100° and because of the repulsive, intramolecular H-H interaction the angle of the minimum configuration is 104.2° [29].

The three-body interactions are responsible for bond length-dependent angular forces and promote mode-mode coupling. To see how these forces arise, consider the gradient of U_3 with respect to the position of atom j, $\mathbf{r}_j$

$$-\frac{\partial U_3}{\partial \mathbf{r}_j} = F_j^{\cos} + F_{ji}^{\exp}. \tag{2}$$

The two force components are represented pictorially in Figure 1(a) and (b). The first term, resulting from the derivative of the cosine term, acts perpendicular to $\mathbf{r}_{ij}$ and depends on the bond length $\|\mathbf{r}_{ij}\|$

$$F_j^{\cos} = 2\left[\cos\theta_{jik} - \cos\theta_{jik}^0\right]^{-1} \left((\hat{\mathbf{r}}_{ij} \cdot \hat{\mathbf{r}}_{ik})\hat{\mathbf{r}}_{ij} - \frac{\hat{\mathbf{r}}_{ik}}{\|\mathbf{r}_{ij}\|} \right) U_3. \tag{3}$$

Unit vectors are denoted by $\hat{\mathbf{x}}$. The second term of the gradient, resulting from the derivative of the exponential screening term, acts parallel to $\mathbf{r}_{ij}$ and is strongly angle-dependent

$$F_{ji}^{\exp} = \gamma_{ij} \frac{e^{\frac{\gamma_{ij}}{\|\mathbf{r}_{ij}\| - r_{ij}^0}}}{\left(\|\mathbf{r}_{ij}\| - r_{ij}^0\right)^2} \hat{\mathbf{r}}_{ij} U_3. \tag{4}$$

When $\gamma_{ij} = 0$ this force is zero. Similar expressions are obtained for particle k. The gradient of the central particle i is the negative sum of the results for particles j and k. Most important to our work is that this feature of the potential promotes coupling between the bond and angular degrees of freedom.

We examine two modifications of the Garofalini *et al*. potential in order to extract the effect of three-body forces on local dynamical instability near potential energy minima and saddles. First, to eliminate the bond length dependence on the HOH angular gradient, the potential is ''unscreened'' (γ_{ij} and γ_{ik} are set to zero), leaving only the first term in the gradient. Figure 1(c) depicts the unscreened forces perpendicular to the OH bond vectors. Second, the bond angle force constant ν_{jik} was adjusted in the ''unscreened'' potential using the condition that the minimum and saddle point configurations have nearly the same energies as their screened counterparts. These modifications to Garofalini *et al*.'s parameters removed the unphysical saddles in the original model.

The isomerization reaction pathways for these modified Garofalini potentials are compared to the original pathways in Figure 2(a). A comparison of the relative ''steepness'' or ''flatness'' of the various saddles demonstrates that our modifications to the model resulted in a more ''pinched'' reaction path, with sharp increases in potential energy around the saddle and gentler increases near the inflection point compared to the original Garofalini H_2O saddle. These modified parameters also impact the normal mode frequencies of the stationary points on these reaction pathways, as shown in Table 1. For reference, also shown in Figure 2(b) is the reaction path of the 12–6 Lennard-Jones trimer, for which the curvature changes sharply in the potential well, but is comparatively flat in the saddle region. The pathway for the Mie trimer, also shown in Figure 2(b), reproduces the curvature of the Garofalini H_2O pathway in Figure 2(a).

The four model triatomics we consider include simple and complicated potential functions, as well as flat and steep isomerization saddles. Though the modifications to Garofalini *et al*.'s potential will likely adversely affect the bulk properties of H_2O, our motivation is to understand the influence of the

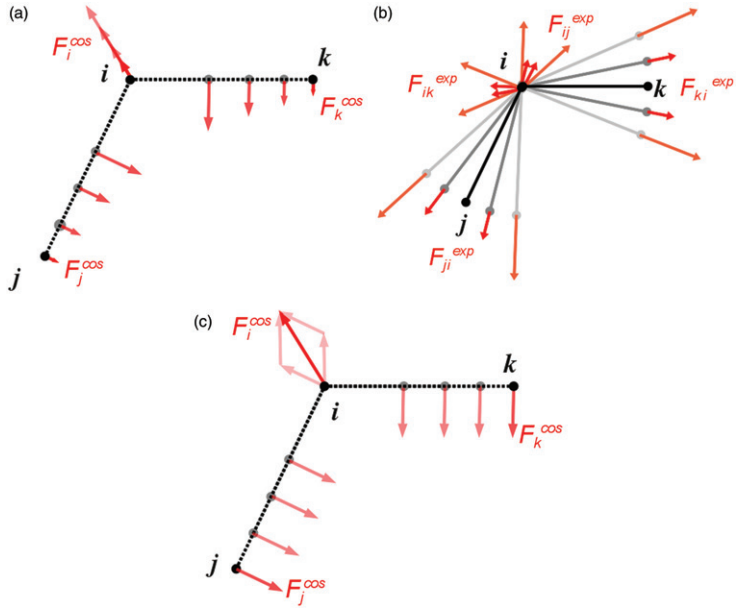

Figure 1. Three-body contributions to the force per particle of Garofalini H_2O. Forces on each particle from (a) the deviations from the ideal HOH angle and (b) the exponential screening of the three-body potential. (c) The forces on each particle with no screening, showing only angle-dependent contributions perpendicular to the OH bond vectors.

various forces on the molecular motion – that is, the dynamics. Of particular interest is to try and separate the effects of the bond length dependent angular forces and the steep H_2O isomerization transition state in the Garofalini model. By turning these forces off and correcting the potential energy barrier height, we can investigate the consequences for several dynamical observables. Similarly, with the 2.1–1.2 Mie potential we can investigate the effect of saddle curvature with a simplified model.

3.2. *Dynamics*

The dynamics of the four models were simulated numerically. Finite-time Lyapunov exponents were computed along the trajectories to quantify the dynamical instability and the local mode action was computed to gauge the degree of mode separability.

3.2.1. *Finite-time Lyapunov exponents*

Water monomer dynamics were simulated at constant total energies just above the linear $D_{\infty h}$ saddle potential energy. As a representative case, we chose the total energy $E = 23.0\,\text{kcal mol}^{-1}$, initially depositing this energy in the bending mode of the global minimum configuration. In all our dynamical simulations, the trajectories were sufficiently long that accumulation of numerical error, the nonlinearity of the potential, and mode-mode coupling led to energy transfer between vibrational modes, including the asymmetric stretch. All trajectories were 100 ns in length, or 10^9 time steps long with a time step size of 0.1 fs. Trajectories were partitioned into time segments of 100 time steps or 10 fs with a 0.1 fs time step. Finite-time Lyapunov exponents were collected from the time segments of these partitioned trajectories to probe the dynamics.

Distributions of the first finite-time Lyapunov exponents are shown in Figure 3 and represent an expansion of our previous results for the dynamics of the original Garofalini H_2O model [24]. These finite-time exponents were collected from a constant total energy trajectory, approximately $1.4\,\text{kcal mol}^{-1}$ above the saddle potential energy and $23\,\text{kcal mol}^{-1}$ above the potential minimum. At this arbitrarily chosen energy, the water molecule is able to isomerize (the highest barrier is $21.57\,\text{kcal mol}^{-1}$ above the minimum) and the configuration accesses the saddle region. Our trajectory simulations were sufficiently long to sample a large number of isomerizations and characterize the phase space flux through the isomerization transition state. Conditional exponent distributions, using the HOH angle averaged over 10 fs time segments (100 time steps), are also shown in Figure 3(a). The cutoff angle of 120° was chosen to separate the exponent populations. Distributions for HOH angles greater than 120° reveal a low-abundance population at large exponent values, $\sim 0.25\,\text{fs}^{-1}$.

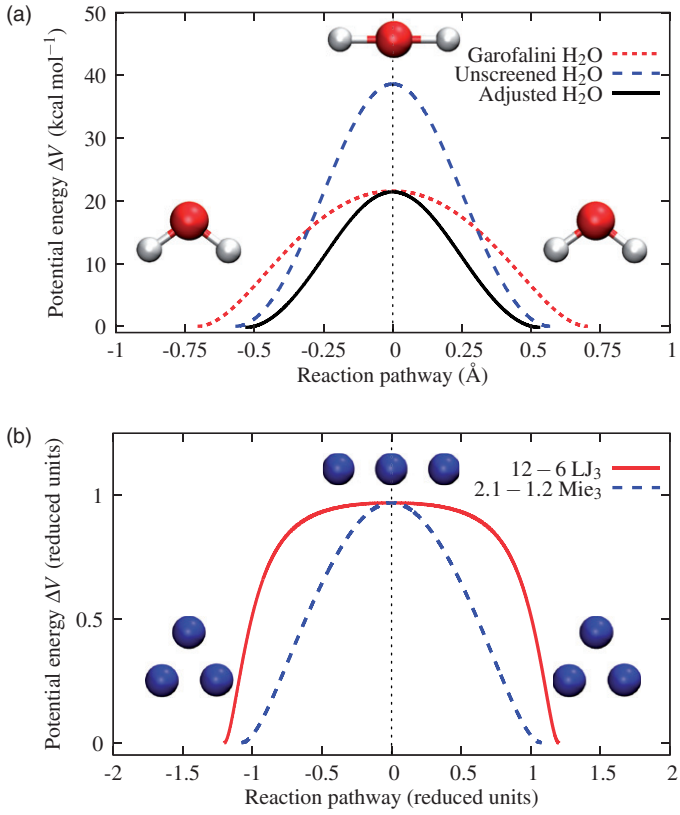

Figure 2. (a) H_2O isomerization pathways for the original Garofalini potential, unscreened three-body potential, and unscreened three-body with an adjusted force constant v_{jik}. With no screening contribution to the three-body term the reaction path is "pinched". (b) Isomerization pathway of the 12–6 Lennard-Jones trimer and the 2.1–1.2 Mie trimer.

This exponent population was not observed from the shorter simulations reported previously.

To better determine the dynamical origin of this population, the exponent distributions were also generated using finite-time averaged kinetic energies (Figure 3b). The population of the smallest exponent values ($\lambda_1 \sim 0.03\ \mathrm{fs}^{-1}$) has the largest abundance. This peak disappears if the kinetic energy is less than a few $\mathrm{kcal\,mol}^{-1}$. Thus, trajectories diverge slower when the kinetic energy is higher than $5\,\mathrm{kcal\,mol}^{-1}$ and comparatively faster when the kinetic energy is lower than $5\,\mathrm{kcal\,mol}^{-1}$. At kinetic energies less than 2 or $5\,\mathrm{kcal\,mol}^{-1}$ two exponent populations at $\lambda_1 \sim 0.12\,\mathrm{fs}^{-1}$ and $0.25\,\mathrm{fs}^{-1}$ are present in the conditional distributions. These peaks were not distinguished previously, but they are both associated with low kinetic energy phase space regions. Based on these results, we can assign the first finite-time Lyapunov exponents in the trimodal distribution as follows: the small exponent population is associated with motion near the potential minimum, and the two larger-exponent populations are associated with the three potential energy saddles (two saddle configurations are permutational isomers, energetically equivalent, with identical potential energy curvatures). Using the abundances of these populations, one of which is half the size of the other, the lower abundance, largest exponent peak is from the index 3 saddle and the smaller (middle) exponent peak is from the index 2 saddles. The abundance of the largest exponent peak is significantly smaller than the other populations because of the small amount of time configurations spend near this highly unstable (index 3) region on the potential energy surface.

For our modified model of H_2O we also found larger finite-time Lyapunov exponents for time segments corresponding to motion near the saddle than those corresponding to motion near the minimum. Figure 4 shows the distribution of the first finite-time Lyapunov exponent (i.e., the exponent associated with the first Gram–Schmidt vector, which in the long run will have the largest positive magnitude) for a trajectory also at a total energy of $23.0\,\mathrm{kcal\,mol}^{-1}$ relative to the minimum, roughly $1.4\,\mathrm{kcal\,mol}^{-1}$ above the saddle.

Table 1. Normal mode vibrational frequencies in cm^{-1} and symmetries for H_2O stationary points with Garofalini's potential, our modifications with no screening of the three-body potential, and from *ab initio* electronic structure calculations at the CCSD/6-311 + G(d, p) level. The Garofalini H_2O linear configuration with $D_{\infty h}$ symmetry has a Hessian index of 3 and the linear configuration with $C_{\infty v}$ has an index of 2. The unscreened Garofalini and CCSD H_2O linear configuration have $D_{\infty h}$ symmetry and a Hessian index of 2. Potential energies ΔV relative to the global minimum potential energy are shown in the last row (kcal mol^{-1}). At the saddle, adjusting the three-body force constant v_{jik} only affects the normal mode in the direction of the reaction path. Only the unscreened, adjusted potential has normal modes with frequencies that have the same order by magnitude as the CCSD frequencies.

Garofalini H_2O

minimum C_{2v}	saddle $D_{\infty\ h}$	saddle $C_{\infty v}$
4077.13 A_1	2665.14 Σ_g^+	4019.43 Σ^+
3986.87 B_2	−1917.66 Σ_u^+	2277.52 Σ^+
1951.57 A_1	−780.19 Π_u	−250.36 Π
$\Delta V = 0$	21.57	17.60

Unscreened Garofalini H_2O

minimum C_{2v}	saddle $D_{\infty h}$
4093.68 A_1	4084.26 Σ_g^+
4075.33 B_2	4275.70 Σ_u^+
1993.56 A_1	−1751.29 Π_u
$\Delta V = 0$	38.61

Unscreened, adjusted Garofalini H_2O

minimum C_{2v}	saddle $D_{\infty h}$
4095.02 A_1	4084.26 Σ_g^+
4095.30 B_2	4275.70 Σ_u^+
1599.01 A_1	−1362.93 Π_u
$\Delta\ V = 0$	21.59

CCSD H_2O

minimum C_{2v}	saddle $D_{\infty h}$
3897.08 A_1	4128.36 Σ_g^+
3999.29 B_2	4515.43 Σ_u^+
1655.45 A_1	−1738.83 Π_u
$\Delta V = 0$	32.97

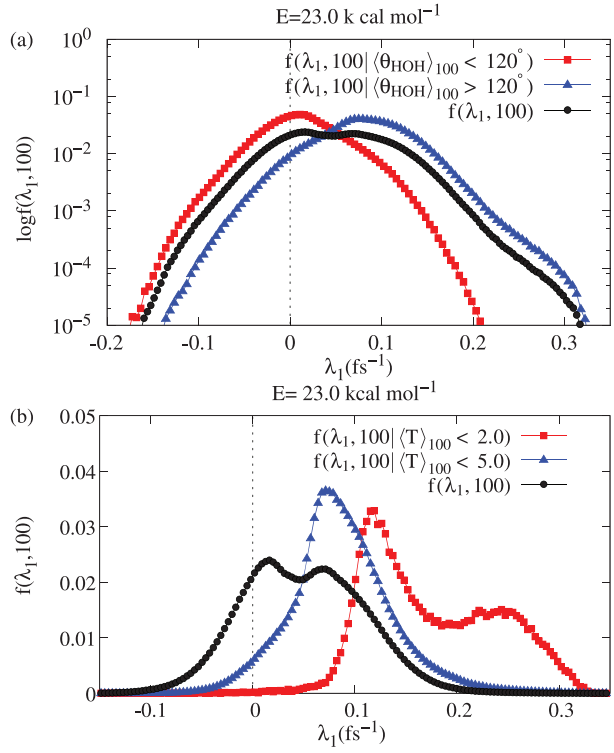

Figure 3. Normalized distributions log $f(\lambda_1, 100)$ and $f(\lambda_1, 100)$ of a representative constant energy H_2O trajectory for the original Garofalini model at $E = 23.0$ kcal mol^{-1}. Conditional distributions using finite-time averages of (a) the HOH angle (degrees) and (b) the kinetic energy T (kcal mol^{-1}), resolving three exponent populations.

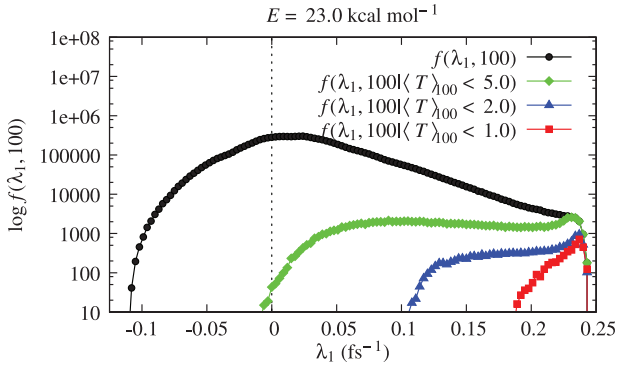

Figure 4. Unnormalized distributions log $f(\lambda_1, 100)$ of one constant energy H_2O trajectory for the unscreened, force constant adjusted Garofalini model. Conditional distributions using the kinetic energy T (kcal mol^{-1}), also averaged over 100 time steps, resolve the exponent populations.

The conditional exponent distributions shown were constructed using trajectory segments in which the kinetic energy is less than 1, 2, and 5 kcal mol^{-1}. (The y-axis is on a logarithmic scale.) These distributions show that smaller kinetic energies correspond to larger finite-time Lyapunov exponents.

The low abundance of the largest-exponent population in this model is also a consequence of the steepness of the saddle and the small amount of time spent there during isomerization. Also, the largest exponents are found when the kinetic energy is low (potential energy is high). Assuming the lowest kinetic

energies correspond to isomerization events, or at least to motion around the saddle, then trajectories diverge most quickly near the saddle. Supporting this interpretation is that the distributions in Figure 4 do not change when adding the condition that the bond angle be greater than 120°. Additional support is given by the normal mode frequencies at the saddle, which are also large for the symmetric (A_1) and asymmetric (B_2) stretches. These distributions agree with our finding that there is only one saddle in the modified model. Though they are first variations in the momentum phase space, the Lyapunov vectors (and exponents) are a response to the rate of change of the associated Lyapunov vector length, in part reflecting changes or fluctuations in potential energy curvature.

The enhanced abundances of the larger magnitude exponent populations in Figure 3 compared to Figure 4 are due to the bond length dependent angular forces in the original Garofalini H_2O model. These forces flatten the saddle of the original Garofalini H_2O, compared to the modified H_2O, shown Figure 2, allowing more time to be spent near the saddle during the time evolution, and leading to the smaller population of large finite-time Lyapunov exponents. In both cases, the potential energy saddles are steep and the motion is more chaotic near the transition state than near the potential minimum.

3.2.2. *Local mode action*

Approximate mode actions are an independent measure of local chaos that also probe mode separability in the H_2O isomerization transition state [15]. Representing the instantaneous atomic positions and momenta of the molecule by $\mathbf{q}(t)$ and $\mathbf{p}(t)$, the approximate action for mode $\hat{\mathbf{u}}_j$ is defined as

$$I_j(n\Delta t) = \sum_{k=1}^{n} p_j(k\Delta t)\Delta q_j(k\Delta t), \tag{5}$$

where p_j and Δq_j are the components of the atomic momenta and position displacements projected onto mode $\hat{\mathbf{u}}_j$

$$p_j(t) = \hat{\mathbf{u}}_j(t) \cdot \mathbf{p}(t), \tag{6}$$

$$\Delta q_j(t) = \hat{\mathbf{u}}_j(t) \cdot [\mathbf{q}(t) - \mathbf{q}(t - \Delta t)]. \tag{7}$$

We set $I_j(t=0)=0$ for each mode. The extent to which each action changes by a constant amount over a time interval measures the separability of the instantaneous modes. For example, better conservation of a local mode action indicates better mode-mode decoupling.

For both Garofalini model parameter sets, trajectories were initiated from nearly linear configurations, that is, close to the $D_{\infty h}$ saddle, by exciting the bending mode of the global minimum configuration. The trajectories were sufficiently long that energy transferred between vibrational modes, including the asymmetric stretch. Thus, for the original Garofalini potential, at later times in the trajectories, the saddle accessed by the dynamics is one of the $C_{\infty v}$ saddles. The many isomerizations undergone in these long trajectories allowed us to investigate the various types of saddle crossings.

An interesting feature of the observed saddle crossings for the original Garofalini H_2O was a significant difference in the magnitude of ΔI_3 during the approach to the saddle compared to the descent from the saddle. As illustrated by Figure 5, the change in magnitude of ΔI_3 before and after isomerization is related to the rate at which isomerization proceeds (as gauged by the HOH angle). This behavior is not observed for any of the other triatomics studied. In fact, the change in ΔI_3 is anticorrelated with the rate at which the HOH angle varies. The origin of this behavior is a barrier-induced crossover of the largest instantaneous normal mode frequency. Traversing the barrier causes a redistribution of energy amongst the vibrational modes, which in turn causes a reordering of the mode frequencies, and the change in ΔI_3. For sufficiently fast isomerizations, the third action was approximately conserved throughout the barrier crossing. These findings suggest that the larger finite-time Lyapunov exponents found at low kinetic energies in "steep" saddles is an indication of the time scale behavior of the mode-mode coupling.

The second action I_2 was not conserved in any of the isomerizations examined (Figure 5b). For fast saddle crossings the first action was generally a smoothly increasing function of time, while slower crossings showed "jumps", suggesting sudden and transient mode-mode coupling. This coupling between the first mode, which is the reactive mode, and the remaining modes is partially responsible for the large finite-time Lyapunov exponents observed at low kinetic energies in H_2O (and H_3O^+, not studied here). However, the potential curvature in different configuration space directions, not just the reaction coordinate, and higher order derivatives also affect mode coupling. The reaction coordinate mode coupling in this model is ultimately a consequence of the bond length dependent angular forces, which also leads to the unphysical $C_{\infty v}$ saddles. Our modifications to the potential parameters eliminated these forces and the additional saddles, made the saddle steeper, and removed this behavior of the local mode actions.

Local mode actions from our modified H_2O purely reflect the effect of curvature in the potential energy function. Specifically, in the unscreened, force constant

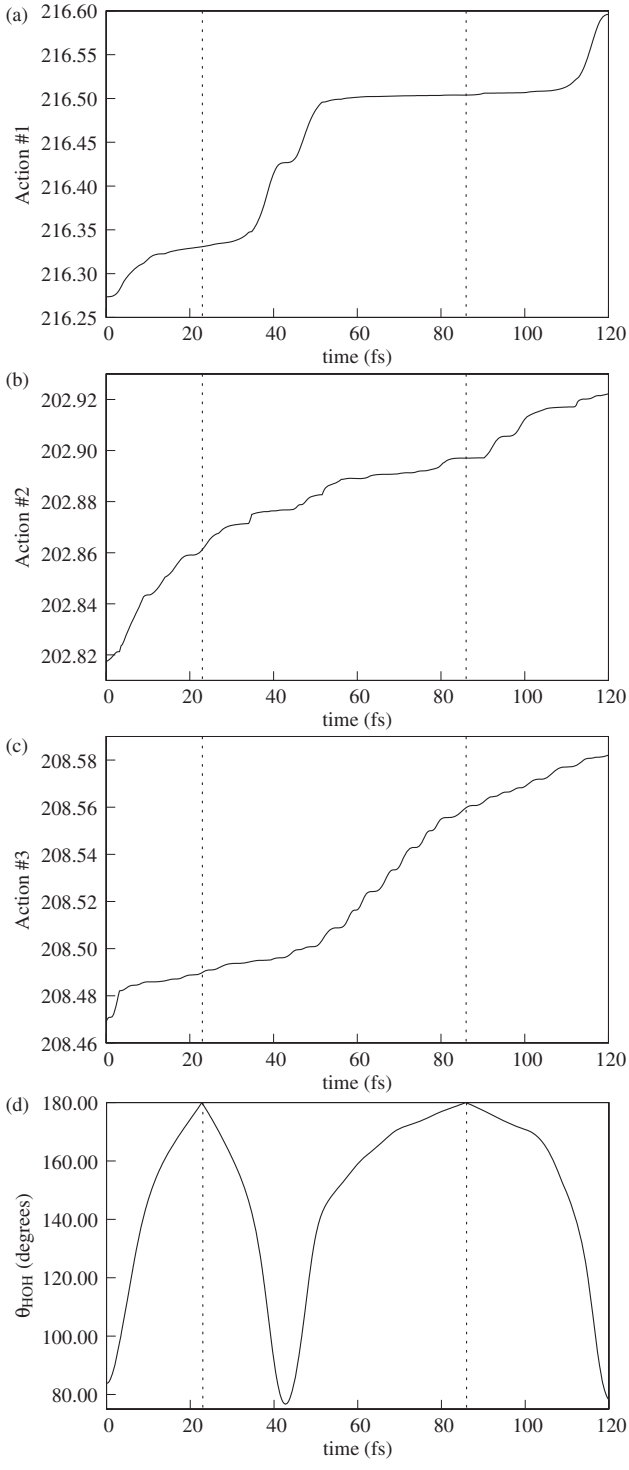

Figure 5. (a)–(c) Approximate local mode actions $I(t)$ versus time, t (fs) from a trajectory segment in which Garofalini H_2O isomerizes twice. (d) The corresponding HOH angles (θ_{HOH} in degrees). ΔI_3 is approximately conserved before and after each isomerization with different magnitudes. The change in ΔI_3 through the saddle depends on the rate of passage, measured by the rate at which the HOH angle changes; small changes in ΔI_3 are observed for faster isomerizations.

adjusted Garofalini H_2O model, the approximate mode actions reveal differences in the mode separability during barrier crossings. We found that some crossings conserve action quite well, but others do not (Figure 6). Interestingly, when ΔI_3 is well conserved, it does not change through the saddle, as it did in the original Garofalini model. Isomerization over the steep barrier is a fast process, and the number of action-conserving isomerizations is sensitive to the total energy and the allocation of the energy amongst the vibrational modes. Generally, we found that with increasing energy fewer isomerizations conserve actions well. The lack of action conservation near the saddle is due to the mixing of instantaneous normal modes. For this set of potential parameters the mixing is between the symmetric and asymmetric stretch-like modes in lower symmetry, as confirmed by a visual inspection of the configurations and the instantaneous

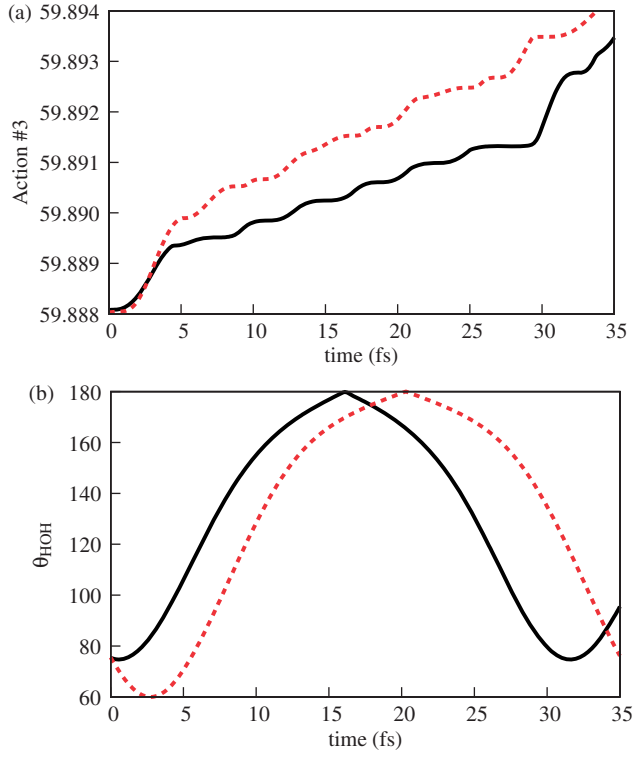

Figure 6. (a) Approximate third local mode action $I_3(t)$ versus time, t (fs) during two different time segments taken from the same trajectory in which H_2O isomerizes. (b) The corresponding HOH angles (θ_{HOH} in degrees) during those trajectory segments. Solid-black curves show ΔI_3 is well conserved and the angle changes quickly during the first time segment. Dashed-red curves show ΔI_3 is poorly conserved and the angle changes slowly during the second time segment. Time segments were 35 fs long and chosen as representative examples of the types of barrier crossings observed during the trajectory.

modes. That is, in contrast to the original Garofalini H_2O, the reaction coordinate probed with the first action is a smooth, usually increasing function of time through the isomerization process, indicating good separation of the reaction coordinate from the remaining modes.

There is a distribution of kinetic energies in the transition state, so it is natural to consider the relationship between the rate of passage through the saddle and action conservation. We found that slow isomerizations (slow changes in the HOH angle) conserve action poorly near the saddle, while isomerizations proceeding quickly conserve the action well, as shown in Figure 6. If an isomerization proceeds slowly, the reaction coordinate contains less kinetic energy than the other modes, which couple more strongly and lead to poor conservation of ΔI_2 and ΔI_3 as a consequence of their extra energy. The reverse is true for fast isomerizations. Examination of the instantaneous normal modes during the trajectory shows switching of modes (caused by the eigenvalue ordering procedure) between symmetric-stretch-like and asymmetric-stretch-like in the saddle region.

Our results for H_2O can be compared with the approximate mode actions for barrier crossings of a 12–6 Lennard-Jones and 2.1–1.2 Mie trimer. In agreement with Hinde *et al.* [15,16], LJ_3 saddle crossings at energies just above the barrier conserve the third mode action well, often for 8–12 periods, and the second mode action only approximately. However, the approximate conservation of these actions degrades as the total energy is raised to the dissociation threshold $V = -1.0\,\varepsilon$. The third mode action is also conserved in isomerizations of the Mie trimer. However, the Mie trimer differs from LJ_3 because of the steepness of the saddle. The features of the third mode action are similar to those obtained for the modified Garofalini H_2O potential shown in Figure 6: ΔI_3 is well conserved in the vicinity of the saddle for fast isomerizations and poorly for slow isomerizations. We can then conclude that the unique properties of the original Garofalini H_2O model saddle crossings – namely the amplified populations of large, positive, first Lyapunov exponents and a change in ΔI_3 upon passing over the saddle – are a consequence of bond length dependent angular forces.

Let us briefly summarize the results for action variables and Lyapunov exponents in flat and steep saddles for three atom systems. ΔI_3 is well conserved when the rate of passage through a *flat* saddle is *slow*. Finite-time Lyapunov exponents are smaller near flat saddles than their connecting potential energy minima. In contrast, ΔI_3 is well conserved when the rate of passage through a *steep* saddle is *fast*. Finite-time Lyapunov exponents are *larger* near steep saddles than their connecting potential energy minima.

4. Conclusions

Our findings indicate the need for a proper account of the anharmonic couplings in theories of transition states. They also provide further insight into the connection between the local curvature of the potential energy landscape and the relative order and disorder of the dynamics that transform reactants into products. Near steep saddles, we have found large exponents and poor action conservation, which correlates with the time scale behavior of mode-mode coupling. The dispersion of trajectories and strong mode coupling found around these transition states contrasts with the collimation of trajectories and mode decoupling found around flatter saddles. These dynamical features are compounded and sometimes amplified by the bond length dependent angular forces in the three-body interactions of Garofalini H_2O. Furthermore, isomerization over steep saddles when these forces are present can redistribute energy amongst the vibrational modes. Interestingly, this intramolecular energy flow is dependent upon how quickly the saddle is traversed and the time spent by the trajectory in the steep saddle.

Acknowledgements

This contribution is dedicated to Dudley Herschbach. J.R.G. acknowledges the computational resources of CamGrid. T.S.H. acknowledges financial support from the Austrian Science Foundation (FWF).

References

[1] W.H. Miller, Faraday Discuss. Chem. Soc. **62**, 40 (1977).
[2] R.A. Marcus, Science **256** (5063), 1523 (1992).
[3] S.K. Gray, S.A. Rice and M.J. Davis, J. Phys. Chem. **90** (16), 3470 (1986).
[4] M.J. Davis and S.K. Gray, J. Chem. Phys. **84** (10), 5389 (1986).
[5] C.C. Martens, M.J. Davis and G.S. Ezra, Chem. Phys. Lett. **142** (6), 519 (1987).
[6] P. Brumer and J.W. Duff, J. Chem. Phys. **65** (9), 3566 (1976).
[7] M. Toda, Phys. Lett. A **48** (5), 335 (1974).
[8] R. Kosloff and S.A. Rice, J. Chem. Phys. **74** (3), 1947 (1981).
[9] H. Fujisaka, Prog. Theor. Phys. **70**, 1264 (1983).
[10] J.P. Eckmann and D. Ruelle, Rev. Mod. Phys. **58** (3), 617 (1985).

[11] C. Amitrano and R.S. Berry, Phys. Rev. Lett. **68** (6), 729 (1992).
[12] C. Amitrano and R.S. Berry, Z. Phys. D **26** (1–4), 388 (1993).
[13] C. Amitrano and R.S. Berry, Phys. Rev. E **47** (5), 3158 (1993).
[14] R.J. Hinde, D.J. Wales and R.S. Berry, J. Chem. Phys. **96** (2), 1376 (1992).
[15] R.J. Hinde and R.S. Berry, J. Chem. Phys. **99** (4), 2942 (1993).
[16] R.J. Hinde and R.S. Berry, Z. Phys. D **26** (1–4), 391 (1993).
[17] D.J. Wales and R.S. Berry, J. Phys. B: At. Mol. Opt. Phys. **24**, L351 (1991).
[18] T. Komatsuzaki and R.S. Berry, J. Chem. Phys. **110** (18), 9160 (1999).
[19] T. Komatsuzaki and R.S. Berry, Proc. Natl. Acad. Sci. USA **98** (14), 7666 (2001).
[20] T. Komatsuzaki and R.S. Berry, Adv. Chem. Phys. **123**, 79 (2003).
[21] H. Waalkens, A. Burbanks and S. Wiggins, J. Chem. Phys. **121** (13), 6207 (2004).
[22] H. Waalkens, R. Schubert and S. Wiggins, Nonlinearity **21** (1), R1 (2008).
[23] J.C. Lorquet, J. Phys. Chem. A **115** (18), 4610 (2011).
[24] J.R. Green, T.S. Hofer, R.S. Berry and D.J. Wales, J. Chem. Phys. **135** (18), 184307 (2011).
[25] G.S. Ezra, Classical trajectory studies of intramolecular dynamics: local mode dynamics, rotation-vibration interaction and the structure of multidimensional phase space, in *Intramolecular Dynamics and Nonlinear Dynamics*, edited by William L. Hase, Vol. 1 (1992), pp. 1–40.
[26] B.G. Sumpter and G.S. Ezra, Chem. Phys. Lett. **142** (3–4), 142 (1987).
[27] R.T. Lawton and M.S. Child, Mol. Phys. **37** (6), 1799 (1979).
[28] R.C. Mayrhofer and E.L. Sibert, Theoretica Chimica Acta **92** (2), 107 (1995).
[29] T.S. Mahadevan and S.H. Garofalini, J. Phys. Chem. B **111** (30), 8919 (2007).
[30] B. Guillot, J. Mol. Liq. **101** (1–3), 219 (2001).
[31] F. Calvo, J. Chem. Phys. **108** (16), 6861 (1998).
[32] E. Yurtsever, Phys. Rev. A **58** (1), 377 (1998).
[33] E. Yurtsever and N. Elmaci, Phys. Rev. A **55** (1), 538 (1997).
[34] G. Mie, Annalen der Physik **316** (8), 657 (1903).
[35] J. Nocedal, Math. Comput. **35** (151), 773 (1980).
[36] L.J. Munro and D.J. Wales, Phys. Rev. B **59**, 3969 (1999).
[37] G. Henkelman and H. Jónsson, J. Chem. Phys. **111** (15), 7010 (1999).
[38] Y. Kumeda, L.J. Munro and D.J. Wales, Chem. Phys. Lett. **341**, 185 (2001).
[39] A. Heyden, A.T. Bell and F.J. Keil, J. Chem. Phys. **123** (22), 224101 (2005).
[40] M. Page and J. James W. McIver, J. Chem. Phys. **88** (2), 922 (1988).
[41] J.R. Green, J. Jellinek and R.S. Berry, Phys. Rev. E **80** (6), 066205 (2009).